Section 9

Development of and studies with coupled ocean-atmosphere models

Progress on an integrated marine Arctic prediction system for METAREAs

*Hal Ritchie, Meteorological Research Division, EC, Dartmouth NS,
Mark Buehner, Meteorological Research Division, EC, Dorval QC
Tom Carrieres, Canadian Ice Service, EC, Ottawa ON
Serge Desjardins, Meteorological Service of Canada – Atlantic, EC, Dartmouth NS
Luc Fillion, Meteorological Research Division, EC, Dorval QC
Edwina Lopes, Meteorological Service of Canada – Ontario, EC, Downsview ON
Pierre Pellerin, Meteorological Research Division, EC, Dorval QC
Gregory Smith, Meteorological Research Division, EC, Dorval QC
Gilles Garric, Mercator-Océan, Toulouse, France

In December 2007 Canada accepted official designation as the Issuing Service for meteorological Marine Safety Information (MSI) in the form of forecasts / warnings and ice bulletins for METAREAs XVII and XVIII as part of the Global Maritime Distress and Safety System (GMDSS). These areas are in the Arctic bordering on Canada. An important part of Environment Canada's involvement is the development of an integrated marine Arctic prediction system and satellite products in support of monitoring and warnings. The integrated marine Arctic prediction system will feed into a highly automated information dissemination system. In particular, our group is working on the development, validation and implementation of marine forecasts with lead times of 1 to 3 days using a regional high resolution coupled multi-component (atmosphere, land, snow, ice, ocean and wave) modelling and data assimilation system to predict near surface atmospheric conditions, sea ice (concentration, thickness, pressure, drift, ice edge), freezing spray, waves and ocean conditions (temperature and currents). The core of the system is an Arctic extension of the highly successful Gulf of St. Lawrence (GSL, Faucher et al. 2010) coupled modelling system, with the GEM (Global Environmental Multi-scale) model as the atmospheric component coupled to the NEMO (Nucleus for European Modelling of the Ocean) ocean model and the CICE ice model. An ice-ocean data assimilation system is being developed in collaboration with Mercator-Océan using their SAM2 system for ocean data assimilation together with the 3DVAR ice analysis system developed at EC (Caya et al. 2010). The following presents recent progress.

The GSL system has been running operationally at the Canadian Meteorological Centre (CMC) since June 2011. This system demonstrated the strong impact that a dynamic sea ice cover (Smith et al., 2012) can have on 48hr atmospheric forecasts leading to large changes in surface air temperature, low-level cloud cover, and precipitation. As a preliminary step for the METAREAs extension of the GSL system, the ocean model developed at the Maurice-Lamontagne Institute is being replaced by NEMO and initial evaluations indicate an equivalent performance.

* *Corresponding author address*: Harold Ritchie, Environment Canada, 45 Alderney Drive, Dartmouth NS, Canada B2Y 2N6; E-mail: Harold.Ritchie@ ec.gc.ca

For the GEM model, a 4DVAR data assimilation system (Tanguay et al. 2011) has replaced the former 3DVAR system and the horizontal resolution of the operational Regional Deterministic Prediction System (RDPS) forecast model has been refined from 15 km to 10 km with a demonstrated improvement in forecasts, particularly over the METAREAs. These improvements were implemented operationally at CMC in October 2012.

The 3DVAR ice concentration analysis system has been operational at CMC since March 2011. Upgrades including assimilation of new passive microwave and scatterometer satellite data and an improved analysis-error standard deviation field for ice concentration were approved for experimental implementation at CMC in January 2013. A stand-alone high-resolution Regional Ice Prediction System (RIPS) for the Arctic has also been developed. This system is initialized using the 3DVAR ice analyses on a 5km North American grid (including the western Arctic) and produces daily 48hr ice forecasts, driven by the RDPS. Verifications demonstrate that RIPS produces a significant gain in forecast skill as compared to persistence of analyses. RIPS was approved for experimental implementation at CMC in March 2013.

A regional Arctic domain operational wave forecast model was implemented at CMC in March 2012. Work is in progress to migrate from the WAM model to the WaveWatch3 model.

Satellite atmospheric products are being developed for the METAREAs including: satellite-model based algorithms to detect fog and icing; data processing to determine cloud versus no cloud areas, stratiform versus convective clouds, and cloud top characteristics; and a synoptic weather-typing approach to quantifying forecast daily snowfall and snow depth over northern Canada.

The integrated METAREAs system is on schedule for full implementation in 2015.

Reference

Caya, A., M. Buehner, and T. Carrieres, 2010: Analysis and forecasting of sea ice conditions with three-dimensional variational data assimilation and a coupled ice-ocean model. J. Atmos. Oceanic Technol. 27, 353-369.

Faucher, M., F. Roy, H. Ritchie, S. Desjardins, C. Fogarty, G. Smith and P. Pellerin, 2010: "Coupled Atmosphere-Ocean-Ice Forecast System for the Gulf of St-Lawrence, Canada", Mercator Ocean Quarterly Newsletter, #38, July 2010, Laurent Crosnier editor, http://www.mercator-ocean.fr/documents/lettre/lettre_38_en.pdf, pages 23-37.

Smith, G.C., F. Roy and B. Brasnett, 2012: Evaluation of an Operational Ice-Ocean Analysis and Forecasting System for the Gulf of St. Lawrence, QJRMS, doi: 10.1002/qj.1982.

Tanguay, M., L. Fillion, E. Lapalme, M. Lajoie, 2011: Four-Dimensional Variational Data Assimilation for the Canadian Regional Deterministic Prediction System. Early online release, *Mon. Wea. Rev.*, July 2011.

The impact of oceanic initial conditions on the simulations of Typhoon Ma-on in 2011

Akiyoshi Wada*

*Meteorological Research Institute, Tsukuba, Ibaraki, 305-0052, JAPAN

awada@mri-jma.go.jp

1. Introduction

Typhoon Ma-on was one of the three typhoons (Typhoons Ma-on, Talas, and Roke) that made landfall in Japan during the 2011 typhoon season. Ma-on was generated at 18.4°N, 156.6°E at 1800 UTC on 11 July 2011. Ma-on moved westward during its developing phase and changed to a northwestward track during its mature phase according to the Regional Specialized Meteorological Center (RSMC) Tokyo best-track data. This study addresses the sensitivity of the difference of oceanic initial conditions due to the difference of the horizontal resolution of oceanic reanalysis data to the simulations of the typhoon. This study also addresses the difference of the impacts between results of a single atmosphere model and an atmosphere-wave-ocean coupled model (Wada et al., 2010).

2. Experimental design

Summary of numerical simulations performed by the atmosphere-wave-ocean coupled model (Wada et al., 2010) is listed in Table1. The coupled model covered nearly a 2800 km x 2100 km computational domain with a horizontal grid spacing of 3 km. The coupled model had 40 vertical levels with variable intervals from 40 m for the near-surface layer to 1180 m for the uppermost layer. The coupled model had maximum height approaching nearly 23 km. The integration time was 120 hours (120 h) with a time step of 8 seconds in the atmospheric part of the coupled model. The time step of the ocean model was six times that of the coupled model and that of the ocean wave model was 10 minutes.

Oceanic initial conditions were obtained from the oceanic reanalysis datasets with horizontal resolutions of 0.1° and 0.5° (Table 1) calculated by the Meteorological Research Institute multivariate ocean variational estimation (MOVE) system (Usui, et al., 2006). Figure 1 displays horizontal distributions of sea surface temperature used in this study. The differences appeared at areas of warm temperature around 22°N, 140°E, south of Japan corresponding to the Kuroshio, and frontal temperature structure north of 30°N.

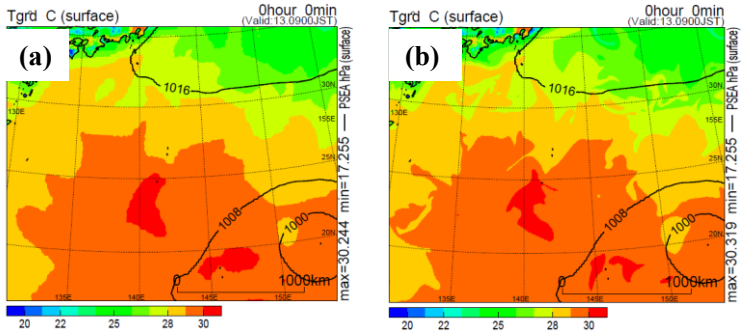

Figure 1 Horizontal distributions of sea surface temperature (shades) and sea-level pressure (contours) at the initial time in experiments (a) A5 and C5, and (b) A1 and C1. The contour interval is 8 hPa.

Table 1 Summary of ocean coupling/noncoupling and horizontal resolution of MOVE data

Experiment	Ocean coupling	Horizontal resolution of MOVE data
A5	NO	0.5°
C5	YES	0.5°
A1	NO	0.1°
C1	YES	0.1°

3. Results

Figure 2a indicates time series of the Regional Specialized Meteorological Center Tokyo (RSMC-Tokyo) best track central pressure and simulated central pressure of Ma-on in experiments A5, A1, C5 and C1 from 0000 UTC on 13 July to 0000 UTC on 19 July in 2011. In experiments A1 and A5, the simulated central pressures were lower than the best track central pressures after 1200 UTC on 14 July. In contrast, the simulated central pressures in experiments C1 and C5 were higher than the best track ones before 1500 UTC on 17 July.

Figure 2b depicts the time series of the central pressure deviations of C1-C5 and A1-A5 during the period of the integration. After 1500 UTC on 17 July, corresponding to the decaying phase (Fig. 2a), variations in the central pressure deviations between experiments A1 and A5 were similar to those between experiments C1 and C5. During the mature phase from 1800 UTC on 16 July to 1500 UTC on 17 July, the central pressure deviations between experiments C1 and C5 little changed, while the simulated central pressure in experiment A1 decreased more rapidly than that in experiment A5 during the time.

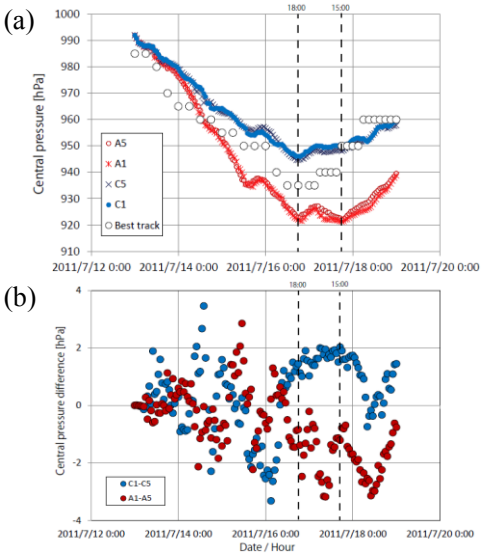

Figure 2 Time series of (a) the best track central pressure (open circles) and simulated central pressure of Ma-on in experiments A5 (red open circles), A1 (red asterisks), C5 (blue cross marks) and C1 (blue closed circles) and (b) central pressure deviations of C1-C5 (blue circles) and A1-A5 (red circles) from 0000 UTC on 13 July to 0000 UTC on 19 July in 2011.

Sea surface cooling induced by a TC can suppress intensification of the TC by delaying the merger of discrete mesovortices (Wada, 2009) indicated by a change in the horizontal distribution of potential vorticity. Figure 3 displayed the horizontal distributions of potential vorticity at 20 m height and sea-level pressure in experiments (a) A5, (b) A1, (c) C5 and (d) C1. In experiments A5 and A1, a ring-like potential vorticity pattern was well simulated at 90 h (1800 UTC on 16 July) with high potential vorticity exceeding 40 PVU (potential vorticity unit). In experiments C5 and C1, we can find a ring-like potential vorticity pattern although the maximum was lower than 30 PVU. All these patterns indicated that the simulated typhoon was mature (Wada, 2009). Compared with the difference between experiments by the atmosphere model alone and the coupled atmosphere-wave ocean model, the difference of the horizontal resolution of MOVE data between 0.5° (Figs. 3a and 3c) and 0.1° (Figs. 3b and 3d) resulted in little difference of the potential vorticity pattern.

Figure 4 depicted time series of mean horizontal specific-humidity (q_v) fluxes within a ring of 60 km widths centered at the radius of maximum wind speed averaged at 1460, 1770, and 2110 m heights, corresponding to 11-13 model levels in all experiments. These heights corresponded to the top of planetary boundary layer where the maximum wind speed appeared.

When Fig. 4 was compared with Fig. 2a, we could find that the variations of mean horizontal q_v fluxes shown in Fig. 4 appeared to be (negatively) correlated with those of simulated central pressures. This suggests that horizontal q_v fluxes could be regarded as a metric for diagnosing simulated central pressures. In particular, the horizontal q_v fluxes clearly decreased from the intensification phase on 15 July due to sea surface cooling. In addition, the deviation in horizontal q_v fluxes kept constant during the mature phase, which was the same characteristic as the deviations of simulated central pressures shown in Fig. 2b.

During the intensification phase, we could find a large variation in horizontal q_v fluxes in experiments C5 and C1 compared with that in experiments A5 and A1. The horizontal distribution of horizontal q_v fluxes showed a wave-number-one pattern and a ring-like pattern of potential vorticity was not formed (not shown). Mesovortices and associated convections within the core of the simulated typhoon may play a crucial role in increasing the q_v fluxes at the top of the planetary boundary layer, affecting the intensification of the simulated typhoon.

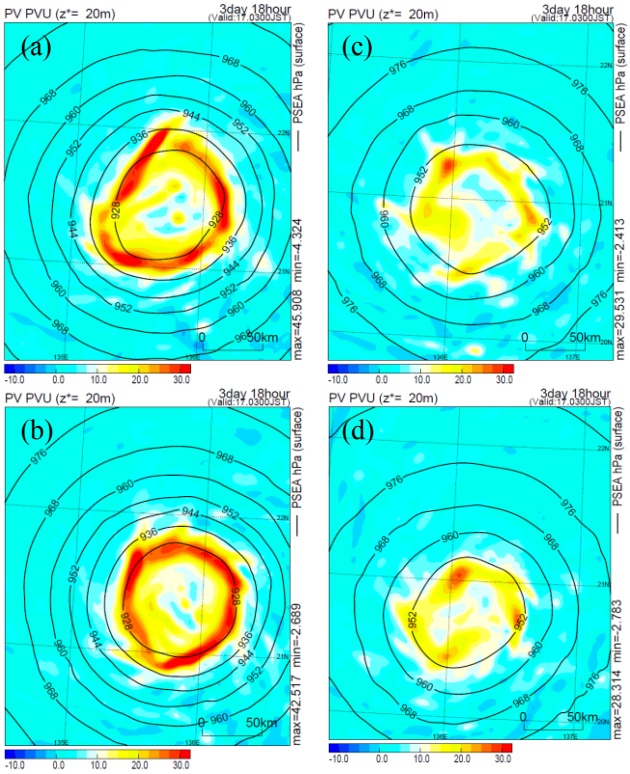

Figure 3 Horizontal distributions of potential vorticity at 20 m height (shades) and sea-level pressure (contours) in experiments (a) A5, (b) A1, (c) C5 and (d) C1. The contour interval is 8 hPa.

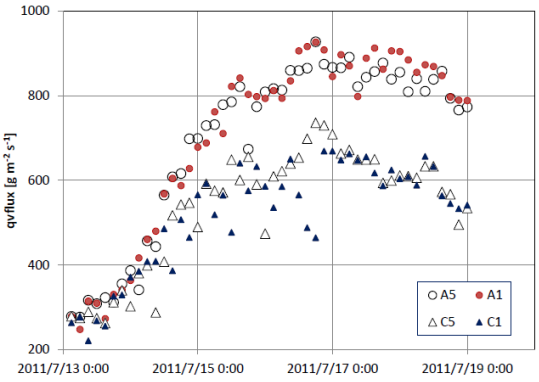

Figure 4 Time series of mean horizontal specific-humidity fluxes within a ring of 60 km widths centered at the radius of maximum wind speed averaged at 1460, 1770, and 2110 m heights, corresponding to 11-13 model levels in all experiments.

4. Discussion and conclusion

This study addresses the impact of the difference of the horizontal resolution of oceanic reanalysis data on the simulations of Ma-on. The impact differs between a single atmosphere model and an atmosphere-wave-ocean coupled model: A higher resolution of oceanic reanalysis data does not always results in a lower simulated central pressure when the coupled atmosphere-wave-ocean model was employed. This study also suggested that horizontal q_v fluxes well corresponds to simulated central pressures. How to determine horizontal q_v fluxes within the inner-core and the relation to oceanic initial conditions will be a subject in the future.

Acknowledgement

This work was supported by the Japan Society for the Promotion of Science (JSPS), Grant-in-Aid for Scientific Research (C) (22540454) and on Innovative Areas (Research in a proposed research area) (23106505).

References

Usui, N., S. Ishizaki, Y. Fujii, H. Tsujino, T. Yasuda, and M. Kamachi (2006), Meteorological Research Institute multivariate ocean variational estimation (MOVE) system: Some early results. *Advances in Space Research*, **37**, 896-822.

Wada, A. (2009). Idealized numerical experiments associated with the intensity and rapid intensification of stationary tropical cyclone-like vortex and its relation to initial sea-surface temperature and vortex-induced sea-surface cooling, *Journal of Geophysical Research*, Vol. **114**, D18111.

Wada, A., N. Kohno and Y. Kawai (2010), Impact of wave-ocean interaction on Typhoon Hai-Tang in 2005, *SOLA*, **6A**, 13-16.

Sensitivity of horizontal resolution and sea spray to the simulations of Typhoon Roke in 2011

Akiyoshi Wada*
*Meteorological Research Institute, Tsukuba, Ibaraki, 305-0052, JAPAN
awada@mri-jma.go.jp

1. Introduction

A previous report of Wada (2012) indicated that the horizontal resolution of 2 km was not enough to simulate the maximum intensity and structural change of Typhoon Roke in 2011 although the nonhydrostatic atmosphere model without ocean coupling well reproduced a rapid decrease in central pressure, 30 hPa in a day. In reality, a rapid intensification of Roke occurred when sea surface cooling was induced by the typhoon. This study addresses the sensitivity of horizontal resolution to the simulations of the typhoon. In addition, the sensitivity of an increase in turbulent heat fluxes due to the effect of sea spray induced by strong winds to the simulations was investigated in order to investigate the impact on the maximum intensity and intensification of simulated Roke.

2. Experimental design

Summary of numerical simulations performed by the atmosphere-wave-ocean coupled model (Wada et al., 2010) is listed in Table1. The coupled model covered nearly a 1600 km x 1600 km computational domain with a horizontal grid spacing of 2 km in experiments A2km and C2km, and that of 1.5km in experiments C1.5km and CSP1.5km. The coupled model had 40 vertical levels with variable intervals from 40 m for the near-surface layer to 1180 m for the uppermost layer.

Table 1 Summary of ocean coupling/noncoupling, horizontal resolution and sea spray parameterization

Experiment	Ocean coupling	Horizontal resolution	Sea spray
A2km	NO	2 km	-
C2km	YES	2 km	-
C1.5km	YES	1.5km	-
CSP1.5km	YES	1.5km	Bao et al.(2000)

The coupled model had maximum height approaching nearly 23 km. The integration time was 84 hours (84 h) with a time step of 6 seconds in the atmospheric part of the coupled model. The time step of the ocean model was six times that of the coupled model. That of the ocean wave model was 10 minutes. Oceanic initial conditions were obtained from the oceanic reanalysis datasets with a horizontal resolution of 0.1º (Table 1) calculated by the Meteorological Research Institute multivariate ocean variational estimation (MOVE) system (Usui, et al., 2006). The sea spray parameterization described in Bao et al. (2000) was used in experiment CSP1.5km.

3. Results

Figure 1 displays time series of the Regional Specialized Meteorological Center Tokyo (RSMC-Tokyo) best track central pressure every six hours and simulated central pressure of Roke every three hours in experiments A2km, C2km, C1.5km and CSP1.5km from 0000 UTC on 18 September to 1200 UTC on 21 September in 2011. The result of sensitivity numerical experiments indicated that the intensification rate simulated in experiment C1.5km, defined as a decrease in central pressures for six hours, was more reasonable to that of the RSMC-Tokyo best track than that simulated in experiment C2km, particularly from 1200 UTC on 19 to 1200 UTC on 20 September. However, simulated central pressures could not reach 940 hPa, the lowest central pressure reported in the RSMC-Tokyo best track data. The lowest simulated central pressure in experiment C1.5km was 949 hPa at 1200 UTC on 20 September, 9 hPa higher than the best track central pressure.

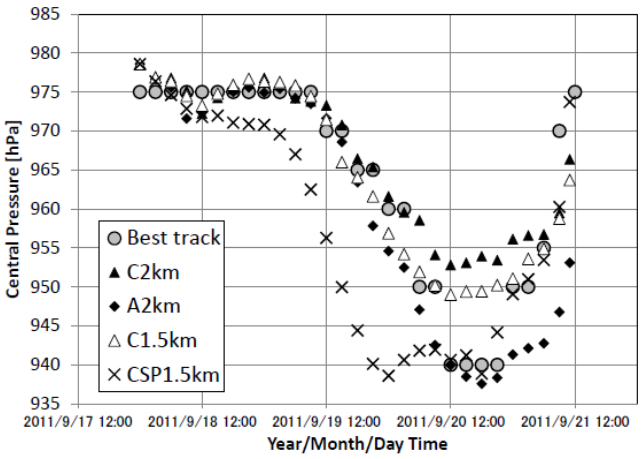

Figure 1 Time series of the best track central pressure and simulated central pressure of Roke in experiments A2km (close diamonds), C2km (close triangles), C1.5km (open triangles) and CSP1.5km (cross marks) from 0000 UTC on 18 September to 1200 UTC on 21 September in 2011.

The experiment CSP1.5km performed by the coupled model incorporating the sea spray parameterization (Bao et al., 2000) indicated more rapid intensification during an earlier integration time in experiment CSP1.5km than in experiments A2km, C2km and C1.5km, which was not consistent with the best track data. The lowest simulated central pressure in experiment CSP1.5km was 938.6 hPa at 0000 UTC on 20 September, which was reasonable to the lowest best track central pressure (940 hPa) although the simulated one appeared 18 hours earlier than the best track one. During the decaying phase of Roke, simulated central pressures tended to be low in experiment A2km and high in experiment C2km, while those were reasonable in experiments C1.5km and CSP1.5km from 0000 UTC to 1200 UTC on 21 September. The results of sensitivity numerical experiments with/without the sea spray parameterization suggest that excessive sea-air turbulent heat fluxes are not necessary for Roke's intensification during an early integration time.

Figure 2 depicted the RSMC-Tokyo best track and simulated positions of Roke every six hours in experiments A2km, C2km, C1.5km and CSP1.5km from 0000 UTC on 18 September to 1200 UTC on 21 September in 2011. No significant differences of simulated positions appeared among experiments A2km, C2km and C1.5km, which had the eastward bias when approaching the Japanese Honshu islands (north of 30°N). The simulated track in experiment CSP1.5km showed more eastward deflections than in experiments A2km, C2km and C1.5km. This indicates that the introduction of sea spray parameterization into the coupled model is not appropriate for the simulation of Roke although the lowest central pressure was well reproduced. In other words, the increase in turbulent heat fluxes beneath Roke due to the effect of sea spray induced by strong winds could not contribute to the improvement of Roke's simulation.

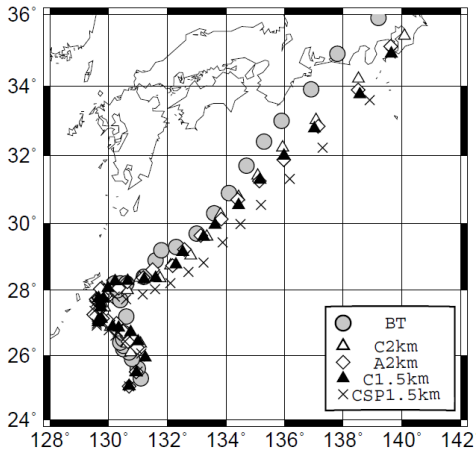

Figure 2 Best track and simulated tracks of Roke in experiments A2km (open diamonds), C2km (open triangles), C1.5km (closed triangles) and CSP1.5km (cross marks) from 0000 UTC on 18 September to 1200 UTC on 21 September in 2011.

Figure 3a displays the horizontal wind speeds at 20 m height in experiment C1.5km at 36 h, when the simulated typhoon began to intensify in experiment C1.5km. The maximum wind speed was ~50 m s^{-1}. The vertical profile of wind speeds (Fig. 3b) indicates that wind speeds were relatively high in the western side where the maximum latent heat flux was relatively high (~488 W m^{-2}: not shown).

Figure 3c displays the horizontal wind speeds at 20 m height in experiment CSP1.5km at 36 h, when the simulated typhoon was intensifying. Interestingly, the maximum wind speed at 20 m height was almost the same as that in experiment C1.5km. The vertical profile of wind speeds (Fig. 3d) indicates a symmetric structure compared with that shown in Fig. 3b. The maximum latent heat flux was ~508 W m^{-2}, which was almost the same as that in experiment C1.5km. Therefore, the effect of sea spray on intensification of simulated Roke appeared in structural change of simulated typhoon, that is, a shrinking process during the intensification.

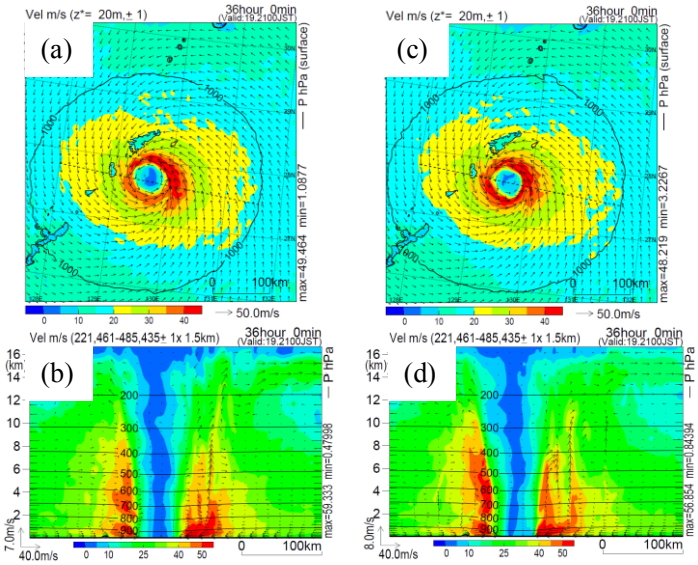

Figure 3 (a) Horizontal distribution of wind speeds at 20 m height in experiments C1.5km and (b) vertical profile of wind speed across the line depicted in Fig. 3a. (c) The horizontal distribution in experiment CSP1.5km. (d) The vertical profile in experiment CSP1.5km. Contours indicate the pressure every 100 Pa.

4. Discussion and conclusion

Even though the sea spray parameterization was incorporated into the coupled atmosphere-ocean model, the present numerical study suggests that the intensity prediction performed by the coupled model could not be improved in all typhoon cases. This result implies that less intensification calculated by the coupled model is not responsible for relatively small turbulent heat fluxes but due to lack of inner-core process of the typhoon. Even though the horizontal resolution is set to 1.5 km, this study shows that the inner-core structure is not always simulated. The influence of atmospheric and oceanic environments on the intensification should be taken into account in the future.

However, high turbulent heat fluxes within the inner core enable the typhoon to intensify at an earlier intensification phase as a trigger. To improve the intensification rate at an early integration, the sea spray parameterization may be effective and should be improved.

Acknowledgement

This work was supported by the Japan Society for the Promotion of Science (JSPS), Grant-in-Aid for Scientific Research (C) (22540454) and on Innovative Areas (Research in a proposed research area) (23106505).

References

Bao, J.-W., J. M. Wilczak, J.-K. Choi, and L. H. Kantha (2000), Numerical simulations of air-sea interaction under high wind conditions using a coupled model: A study of hurricane development. *Mon. Wea. Rev.*, **128**, 2190-2210.

Usui, N., S. Ishizaki, Y. Fujii, H. Tsujino, T. Yasuda, and M. Kamachi (2006), Meteorological Research Institute multivariate ocean variational estimation (MOVE) system: Some early results. *Advances in Space Research*, **37**, 896-822.

Wada, A., N. Kohno and Y. Kawai (2010), Impact of wave-ocean interaction on Typhoon Hai-Tang in 2005, *SOLA*, **6A**, 13-16.

Wada, A. (2012), Rapid intensification of Typhoon Roke in 2011. *CAS/JSC WGNE Res. Activities in Atm. and Oceanic Modelling*, **42**, 9.05-9.06.

Lagged simulations of the oceanic initial condition for Typhoon Choi-wan (2009)

Akiyoshi Wada
*Meteorological Research Institute, Tsukuba, Ibaraki, 305-0052, JAPAN
awada@mri-jma.go.jp

1. Introduction

On 19 September 2009, the eye of Typhoon Choi-Wan passed ~40 km to the southeast of the Kuroshio Extension Observatory (KEO) surface mooring, located at 32.3ºN, 144.5ºE. Bond et al. (2011) reported the large variation (~50 μatm) in ΔpCO_2 (=pCO_2^{sea}-pCO_2^{air}: surface oceanic partial CO_2 minus surface atmospheric partial CO_2) observed during the typhoon passage. Nearly forty percent of ΔpCO_2 (~ 20 μatm) was explained by rapidly falling pCO_2^{air} during the passage. Thus, approximately sixty percent of ΔpCO_2 should be explained by a rapid increase of surface pCO_2^{sea} during the typhoon passage. However, the atmosphere-wave-ocean model could not fully simulate the rapid increase of surface pCO_2^{sea} under given atmospheric and oceanic initial conditions. Excessive sea-surface cooling and resultant low surface pCO_2^{sea} compared with observations at the KEO surface mooring may be caused due to uncertainties of atmospheric and oceanic initial conditions. In order to understand the effect of oceanic initial conditions on the simulation of the oceanic response to Choi-wan (2009), lagged ensemble numerical simulations for Choi-wan associated with the oceanic initial condition were carried out by the atmosphere-wave-ocean coupled model providing daily oceanic reanalysis data individually from 12 to 25 September in 2009. The daily oceanic reanalysis data were calculated by the Meteorological Research Institute Ocean Variational Estimation system (MOVE: Usui et al. (2006)).

2. Experiment design

The lagged ensemble numerical simulations were performed by a nonhydrostatic atmosphere model coupled with the multilayer ocean model, the ocean wave model and the oceanic carbon equilibrium scheme. The model specification was as follows: The computational domain was 3240 km x 3960 km with a horizontal grid spacing of 6 km. The model had 40 vertical levels with variable intervals from 40 m for the lowermost (near-surface) layer to 1180 m for the uppermost layer. The model had maximum height approaching nearly 23 km. The time step of the nonhydrostatic model was 20 seconds. The length of the time step of the ocean model was six times (that is 120 seconds) that of the atmosphere model. The time step of the ocean wave model was 10 minutes. Each initial depth of the oceanic mixed layer was determined every oceanic reanalysis data from 12 to 25 September in 2009, by assuming a difference in the value of density from the surface of no more than 0.25 kg m^{-3} and the depth of the mixed layer was limited to 200 m. The base of the thermocline was limited to 600 m and water depth was limited to 2000 m.

The integration hour was 96 hours. However, we used the results of numerical simulations from the initial time to 84 hours. The lateral boundary condition with the width of lateral boundary sponge layer of 1080 km (180 grids) was changed every six hours. The momentum, sensible and latent heat fluxes were given to the ocean model. It should be noted that the normalization of dissolved inorganic carbon (DIC) and total alkalinity (ALK) to a salinity of 34.1 from a salinity of 35.0 was done at the initial time of numerical simulations. In addition, ALK at the initial time were determined from the following formula.

$$ALK_{init} = \begin{cases} 2500.9T_i^{-0.0029} & T > 18.0 \\ 2299.818 & T \le 18.0 \end{cases}, \quad (1)$$

where T_i is water temperature at the i-th level of the multilayer ocean model. DIC at the initial time are determined from the formula as described in Wada et al. (2011).

The KEO reference station is a highly instrumented moored buoy located at 32.3ºN, 144.5ºE, in the recirculation gyre south of the Kuroshio Extension (Cronin et al., 2008). In this study, we use data from the KEO mooring, including hourly meteorological data, hourly sea-surface temperature, sea-surface salinity and 3 hourly pCO_2 from a Moored Autonomous pCO_2 system (Bond et al., 2011) for validation of the ensemble numerical simulation results.

3. Results

3.1. Sea-level pressure and surface air temperature

Figure 1 shows time series of sea-level pressure (Fig.1a) and surface air temperature (Fig.1b) observed at the KEO mooring and simulated at the corresponding grid to the KEO buoy site. Lowest simulated sea-level pressure appeared three hours after lowest best-track one. Simulated air temperatures were higher just before the passage of simulated typhoon than the observations, and were lower after the passage.

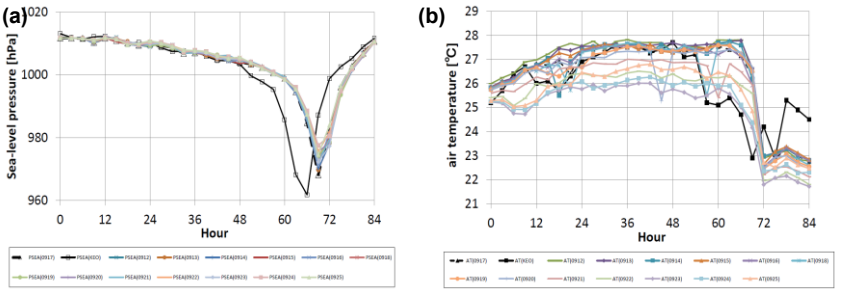

Fig.1 Time series of (a) sea-level pressure and (b) surface air temperature observed at the KEO mooring (black line) and simulations

3.2 Oceanic ingradients

Figure 2 shows time series of sea-surface temperature (Fig.2a) and sea-surface salinity (Fig.2b) observed at the KEO mooring and simulated at the corresponding grid of the KEO buoy site. Simulated sea-surface temperature varied at the initial time with a range of 26.5 ˚C to 28 ˚C. Excessive sea-surface cooling occurred after the passage of the typhoon in all simulations compared to the observations. In contrast, simulated sea-surface salinity showed that the evolution quite differed among oceanic initial conditions from 12 to 25 September in 2009.

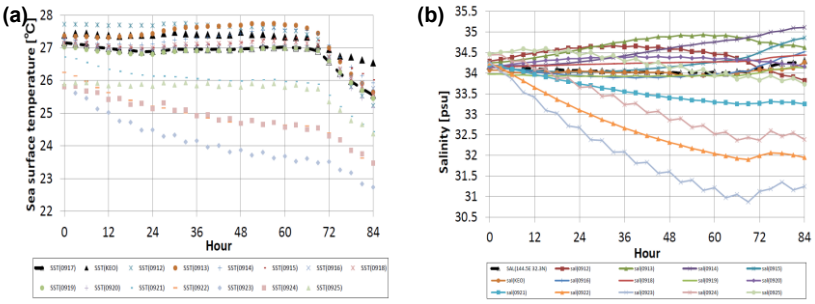

Fig.2 Same as Fig. 1 except for (a) sea-surface temperature and (b) sea-surface salinity.

Figure 3 shows time series of surface pCO_2^{sea} (Fig. 3a) and that normalized to a temperature of 29 ˚C (Fig. 3b). The evolution of surface pCO_2^{sea} was closely related to that of sea-surface temperature (Fig. 2a): Simulated surface pCO_2^{sea} rapidly decreased after the passage.

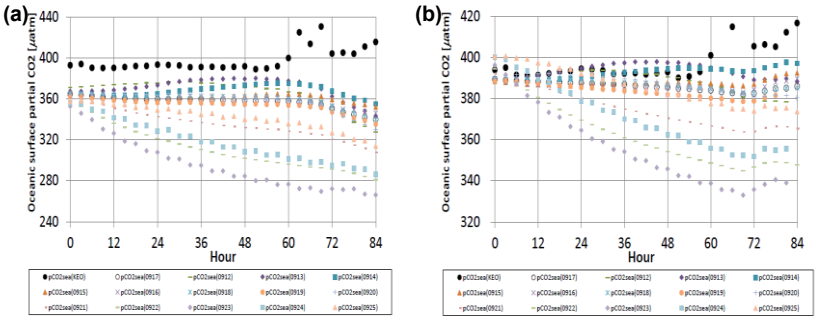

Fig.3 Same as Fig. 1 except for (a) surface pCO_2^{sea} and (b) surface pCO_2^{sea} normalized to a temperature of 29 ˚C.

The evolution of surface pCO_2^{sea} normalized to a temperature of 29 ˚C showed that normalized surface pCO_2^{sea} increased after the passage of simulated Choi-wan. The evolution of surface pCO_2^{sea} normalized to a temperature of 29 ˚C was similar to that of sea-surface salinity. In Fig. 3, both the evolutions of surface pCO_2^{sea} and the normalized one quite differed from those of observation. However, some of simulations partly captured a variation in surface pCO_2^{sea} and the normalized one except the rapid variation during the passage of the typhoon (Fig. 3a). Pre-existing oceanic condition (before 17 September in 2009) would be favorable to simulate a variation in surface pCO_2^{sea} and post-existing oceanic condition (after 20 September in 2009) would be necessary to simulate the increases in sea-surface salinity and the normalized surface pCO_2^{sea} after the passage of the typhoon.

4. Conclusions

Lagged ensemble simulations for the typhoon associated with the oceanic initial condition were carried out by the atmosphere-wave-ocean coupled model providing daily oceanic reanalysis data from 12 to 25 September in 2009 as oceanic initial conditions in order to understand the effect of oceanic initial conditions on the simulation of the oceanic response to Typhoon Choi-wan in 2009. We could find the impact of the oceanic initial condition on simulated sea-level pressure and surface air-temperature only during the passage of the typhoon. In contrast, we could clearly find the impact on simulated sea-surface temperature, sea-surface salinity, surface pCO_2^{sea} and that normalized to a temperature of 29 ˚C during and after the passage of the typhoon. In addition, some of simulations could partly capture a variation in surface pCO_2^{sea} and the normalized one after the passage of the typhoon even though we find no rapid variation during the passage of the typhoon.

This study suggests that oceanic initial condition can affect the evolution of surface pCO_2^{sea} by passage of the typhoon. In addition, the results of validation using the observations at the KEO mooring imply that the three-dimensional ocean circulation model will be required to simulate the variation in oceanic ingredients by passage of the typhoon under given atmospheric conditions. Moreover, atmospheric ensemble approach will be needed to estimate uncertainties of atmospheric conditions, including the improvement of track simulations. These are future subjects in this study.

Acknowledgement

This work was supported by the Japan Society for the Promotion of Science (JSPS), Grant-in-Aid for Scientific Research (C) (22540454) and on Innovative Areas (Research in a proposed research area) (23106505).

References

Bond, N. A., M. F. Cronin, C. Sabine, Y. Kawai, H. Ichikawa, P. Freitag, and K. Ronnholm (2011), Upper ocean response to Typhoon Choi-wan as measured by the Kuroshio Extension Observatory mooring, *J. Geophys., Res*., 116, C02031.

Cronin, M. F., C. Meinig, C. L. Sabine, H. Ichikawa, and H. Tomita (2008), Surface mooring network in the Kuroshio Extension, IEEE Syst. J., 2(3), 424–430.

Usui, N., Ishizaki S., Fujii Y., Tsujino H., Yasuda T., and Kamachi M. (2006), Meteorological Research Institute multivariate ocean variational estimation (MOVE) system: Some early results. *Advances in Space Research*, **37**, 896-822.

Wada, A., 2012: *Numerical study on the effect of the ocean on tropical-cyclone intensity and structural change*, Atmospheric Models. (Ed. I. Yucel) InTech, in press.

Wada, A., T. Midorikawa, M. Ishii, and T. Motoi (2011), Carbon system changes in the East China Sea induced by Typhoons Tina and Winnie in 1997, *J. Geophys. Res.*, **116**, C07014.

Impacts of surface roughness lengths on axisymmetrically mean structure of Typhoon Fanapi (2010)

Akiyoshi Wada
*Meteorological Research Institute, Tsukuba, Ibaraki, 305-0052, JAPAN
*awada@mri-jma.go.jp

1. Introduction

Ocean waves cause variation in surface roughness lengths over the ocean particularly during the passage of tropical cyclones (TC). Wada and Kohno (2012) investigated the impact of surface roughness lengths on TC simulations. They concluded that the impact on TC track simulations was negligibly small but that on simulated central pressure was ~10 hPa during the intensification of simulated Typhoon Fanapi in 2010. The exchange coefficient for the momentum flux associated with surface roughness lengths plays an important role in estimation of the effect of surface friction on inward angular momentum transport, because surface friction is considered to affect tangential winds and radial inflow and thereby secondary circulation. However, Wada and Kohno (2012) did not address impacts of surface roughness lengths on the axisymmetrical structure of the typhoon.

In order to understand the effect of surface roughness lengths on the axisymmetrical structure of simulated typhoon, this study performed numerical simulations for Typhoon Fanapi (2010) using a nonhydrostatic atmosphere model coupled with an ocean wave model and a multi-layer ocean model (Wada et al., 2010) with a similar experimental design to Wada and Kohno (2012). The surface roughness length calculated by the coupled model is determined by the following five methods, respectively; functions of wave-induced stress (Janssen, 1991), wave age (Smith, 1992), wave steepness (Taylor and Yelland, 2001), the assumption of Charnock constant (Charnock, 1955), and drag coefficients depending on 10-m wind speed (Kondo, 1975).

2. Experimental design

Five numerical simulations were performed for Fanapi by using the coupled model incorporating each surface roughness length scheme mentioned above (Table 1). The coupled model covered a 2000 km x 1800 km computational domain with a horizontal grid spacing of 2 km. The coupled model had 40 vertical levels with variable intervals from 40 m for the near-surface layer to 1180 m for the uppermost layer. The coupled model had maximum height approaching ~23 km. The integration time was 72 hours with a time step of 6 s in the atmosphere model.

Oceanic initial conditions were obtained from the oceanic reanalysis datasets with horizontal resolution of 0.1°, calculated by the Meteorological Research Institute multivariate ocean variational estimation (MOVE) system (Usui, et al., 2006).

In the present study, the parameterization of ice nucleation proposed by Murakami (1990) was used instead of that of Meyer et al. (1992). Figure 1 shows time series of best-track central pressure and five simulated central pressures for Fanapi. The results of simulated central pressures slightly differed from those of Wada and Kohno (2012).

Table 1 List of numerical simulations, surface roughness scheme used, and horizontal resolution of oceanic initial condition.

Experiment		Surface roughness scheme	Horizontal resolution of MOVE
CH	CH1	Charnock (1955)	0.1°
JA	JA1	Janssen (1991)	0.1°
KO	KO1	Kondo (1975)	0.1°
SM	SM1	Smith (1992)	0.1°
TY	TY1	Taylor and Yelland (2001)	0.1°

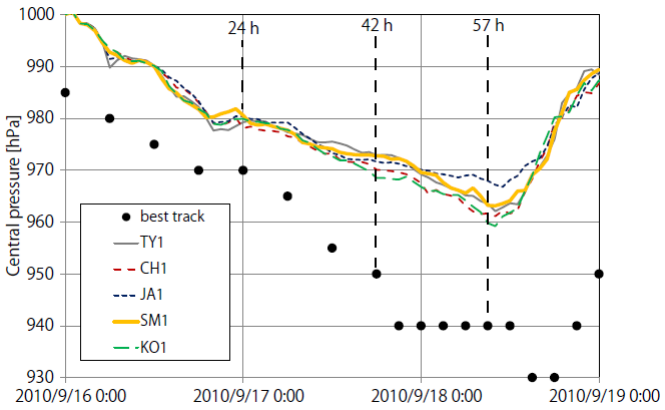

Figure 1 Time series of best-track central pressure and simulated ones.

3. Results

Figure 2 displays vertical profiles of axisymmetrically mean radial flow (contours) averaged among the five experiments with the standard deviations (shades) at 24 h (left panel), 42 h (middle panel) and 57 h (right panel). High standard deviations indicate that the impact of surface roughness lengths is high so that mean value is not significant. In other words, variation in surface roughness lengths is sensitive to axisymmetrically mean structure where the standard deviation is high. Figure 2 indicates that the inflow layer within the surface boundary layer is little affected by variation in surface roughness lengths, whereas outflows above the inflow layer and around 8000 m heights are sensitive to the variation. During the early intensification (24 h), axisymmetrically mean inflow layer relatively was thin and mean outflow above the mean inflow layer around the radius of 50 km was small. During the intensification phase (42 h), mean inflow reveals intrusion into the TC center. Axisymmetrically mean outflow above the mean inflow layer became high with high standard deviations around the radius of 50 km. During the mature phase (57 h), the mean inflow layer became thickest of the three integration times, indicating the occurrence of supergradient flow at the inner edge of mean inflow where high standard deviations appear. High standard deviations also appear along the inner side of the eyewall and around 8000 – 10000 m heights. These areas with high standard deviations correspond to the location of the secondary circulation.

Figure 3 displays vertical profiles of axisymmetrically mean equivalent potential temperature (contours) averaged among five experiments shown in Table 1 with the standard deviations (shades) at 24 h (left panel), 42 h (middle panel) and 57 h (right panel). During the early intensification (24 h), areas of higher mean equivalent potential temperature than the surrounding were relatively small around the TC center and the horizontal gradient was relatively small. During the intensification phase (42 h), the horizontal gradient became sharp around the radius of 50 -100 km and equivalent potential temperature became high. During the mature phase (57 h), the horizontal gradient became sharpest. The standard deviations of equivalent potential temperature were high above the inner edge of the inflow layer and around 8000 – 10000 m heights.

Figure 4 displays vertical profiles of axisymmetrically mean stability multiplying vertical velocity (contours) averaged among five experiments shown in Table 1 with the standard deviations (shades) at 24 h (left panel), 42 h (middle panel) and 57 h (right panel). Because high value of stability multiplying vertical velocity indicates high adiabatic cooling, Figure 4 reveals that adiabatic cooling within the eyewall is highly sensitive to variation in surface roughness lengths particularly during the mature phase (57 h). The sensitivity is also related to the process of the secondary circulation.

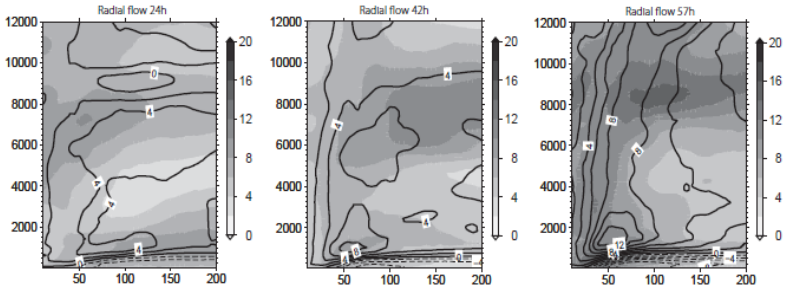

Figure 2 Vertical profiles of axisymmertically mean radial flow (contours) averaged among five experiments shown in Table 1 and the standard deviations (shades) at 24 h (left panel), 42 h (middle panel) and 57 h (right panel).

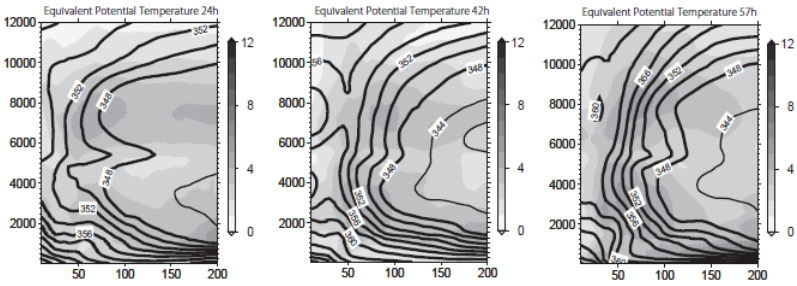

Figure 3 Same as Fig. 2 except for equivalent potential temperature.

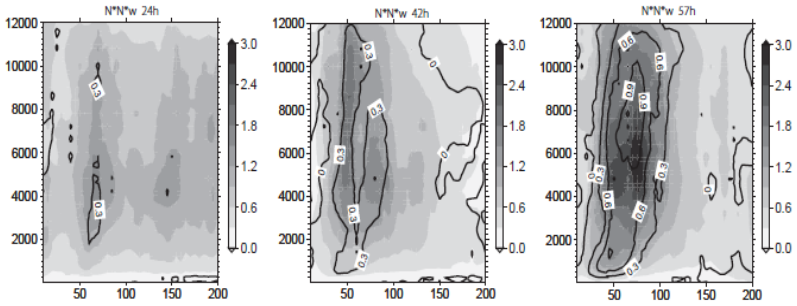

Figure 4 Same as Fig. 2 except for stability multiplying vertical velocity.

4. Discussion and conclusion

The impact of variation in surface roughness lengths on axisymmetrically mean structure of simulated Typhoon Fanapi (2010) appeared remarkably in the process of the secondary circulation at areas of supergradient inflow and associated outflow above the inner edge of the inflow layer, along the eyewall and around 8000 – 10000 m heights. It is noted that the impact on the inflow layer in the surface (frictional) boundary layer is relatively small although that on tangential flow is relatively high (not shown). The result may imply that the secondary circulation is not always forced by surface frictional inflow appeared in the surface boundary layer. We will further investigate the impact on the axisymmetrical structures of specific humidity and its horizontal flux in the future in order to understand the impact on microphysics associated with intensification process of simulated Fanapi.

Acknowledgements

This work was supported by the Japan Society for the Promotion of Science (JSPS), Grant-in-Aid for Scientific Research (C) (22540454) and on Innovative Areas (Research in a proposed research area) (23106505).

References

Charnock, H. (1955), Wind stress on a water surface, *Quart. J. Roy. Meteor. Soc.*, **81**, 639-640.

Jansen, P. A. E. M. (1991), Quasi-linear theory of wind-wave generation applied to wave forecasting, *J. Phys. Oceanogr.*, **21**, 1631-1642.

Kondo, J. (1975), Air-sea bulk transfer coefficients in diabatic conditions. *Bound. Layer Meteor.*, **9**, 91-112.

Louis, J. F., M. Tiedtke, and J. F. Geleyn (1982), A short history of the operational PBL parameterization at ECMWF. Proc. *Workshop on Planetary Boundary Layer Parameterization, Reading, United Kingdom*, ECMWF, 59–79.

Meyer, M. P., P. J. DeMott, and W. R. Cotton (1992), New primary ice-nucleation parameterizations in an explicit cloud model. *J. Appl. Meteor.*, 31, 708-721.

Murakami, M. (1990), Numerical modeling of dynamical and microphysical evolution of an isolated convective cloud – the 19 July 1981 CCOPE cloud. *J. Meteor. Soc. Japan*, 68, 107-128.

Smith, S. D., R. J. Anderson, W. A. Oost, C. Kraan, N. Maat, J. Decosmo, K. B. Katsaros, K. L. Davidson, K. Bumke, L. Hasse, and H. M. Chadwick (1992), The HEXOS results. *Boundary-Layer Meteorol.*, **60**, 109-142.

Taylor, P. K., and M. J. Yelland (2001), The dependence of sea surface roughness on the height and steepness of the waves. *J. Phys. Oceanogr.*, **31**, 572-590.

Usui, N., S. Ishizaki, Y. Fujii, H. Tsujino, T. Yasuda, and M. Kamachi (2006), Meteorological Research Institute multivariate ocean variational estimation (MOVE) system: Some early results. *Advances in Space Research*, **37**, 896-822.

Wada, A., N. Kohno and Y. Kawai (2010), Impact of wave-ocean interaction on Typhoon Hai-Tang in 2005, *SOLA*, **6A**, 13-16.

Wada, A. and N. Kohno (2012), Impact of surface roughness lengths on simulations of Typhoon Fanapi (2010), *CAS/JSC WGNE Res. Activ. Atmos. Oceanic. Modell.* **42**, 9-11

Effect of Talas-induced sea-surface cooling on the generation of a subsequent typhoon

Akiyoshi Wada*
*Meteorological Research Institute, Tsukuba, Ibaraki, 305-0052, JAPAN
awada@mri-jma.go.jp

1. Introduction

This study focuses on the effect of sea surface cooling induced by Typhoon Talas in 2011 on the genesis and development of a subsequent typhoon. In fact, a tropical depression was detected around 21.3°N, 149.8°E at 0000 UTC on 2 September and thereafter Typhoon Noru was generated at 22.2°N, 150.3°E at 1200 UTC on 3 September in 2011. The genesis location was east of the track of Talas. After the genesis, Noru moved northward, away from the Talas's track. This study performed numerical simulations using a nonhydrostatic atmosphere model coupled with an ocean wave model and a multi-layer ocean model (Wada et al., 2010) to investigate the effect.

2. Experimental design

Summary of numerical simulations performed by the atmosphere-wave-ocean coupled model is listed in Table 1. The coupled model covered nearly a 4300 km x 5000 km computational domain with a horizontal grid spacing of 6 km. The coupled model had 40 vertical levels with variable intervals from 40 m for the near-surface layer to 1180 m for the uppermost layer. The coupled model had maximum height approaching nearly 23 km. The integration time was 384 hours (384 h) with a time step of 20 seconds in the atmospheric part of the coupled model. The time step of the ocean model was six times that of the coupled model. That of the ocean wave model was 10 minutes.

Table 1 Summary of abbreviation of numerical experiment, ocean coupling/noncoupling and parameters of Rayleigh damping width associated with the lateral boundary condition used in this study.

Experiment	Ocean coupling	Rayleigh damping width
A15	NO	15
C15	YES	15
A50	NO	50
C50	YES	50

This study performed the sensitivity numerical experiments of Rayleigh damping width associated with the lateral boundary condition in order to investigate the sensitivity of lateral boundary condition provided every six hours to the generation and development of a subsequent typhoon. Oceanic initial conditions were obtained from the oceanic reanalysis datasets with horizontal resolutions of 0.1º calculated by the Meteorological Research Institute multivariate ocean variational estimation (MOVE) system (Usui, et al., 2006). The surface roughness length calculated by the coupled model was derived from the formulation based on wave steepness (Taylor and Yelland, 2001).

3. Results and discussions

Results of track simulations and the best track of Talas (Fig. 1a) and Noru (Fig. 1b) indicate that the Rayleigh damping width associated with the lateral boundary condition clearly affected the track of simulated Talas irrespective of the effect of sea surface cooling (Fig. 1a). In experiments A50 and C50, simulated Talas tended to move westward when the best-track typhoon moved to northward (Wada, 2012). In contrast, the westward movement of the simulated typhoon north of 28°N appeared to cause errors compared with the best track in experiments A15 and C15. Sea surface cooling induced by simulated Talas affected the track simulations after 138 h when the center position of the typhoon was north of 30°N.

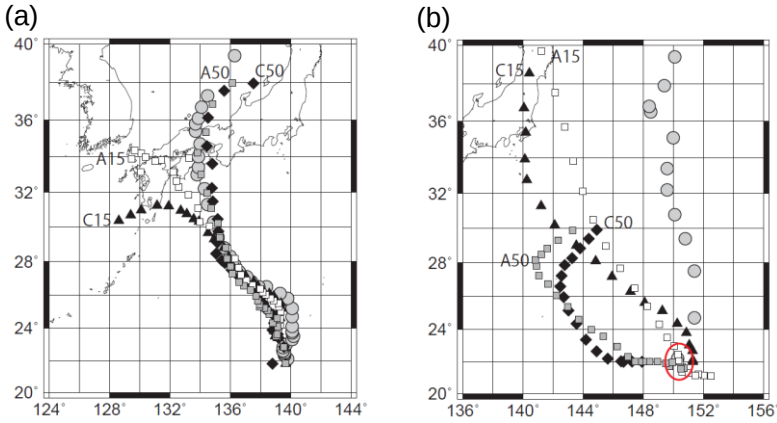

Figure 1 (a) Best track and simulated tracks of Talas in experiments A15（open squares）, C15(close triangles), A50(gray squares), and C50(close diamonds). (b) Same as Fig.1(a) except those of Noru. The end of simulated track in Naru's case is 1200 UTC on 6 September. A red circle indicates the genesis location of Naru according to the Regional

The locations of simulated Naru shown in Fig. 1b were determined from the positions that the simulated central pressure was lower than 1000 hPa with the maximum wind speed exceeding 34 knot. These criteria correspond to the phase of 'typhoon'. The results of simulations show that the locations of all simulated tropical typhoons appeared at 1800 UTC on 30 August (experiment A15), at 0600 UTC on 31 August (experiment A50), at 0000 UTC on 1 September (experiment 15) and at 0600 UTC on 2 September (experiment C50) around 22°N, 150°E. All appearance times were earlier than the time of best-track tropical cyclone genesis, at 1200 UTC on 3 September (A red circle in Fig.1b). This suggests that typhoon-induced sea surface cooling contributes to delaying of the genesis of a subsequent simulated typhoon. In addition, the parameter of lateral boundary sponge layer plays a crucial role in simulating the tracks of Talas and Nari. In fact, the simulated tracks in Fig. 1b quite differed among the four experiments. In this study, the parameter 50, corresponding to the width of 300 km, seems to be more reasonable to simulate the two typhoons than the parameter 15.

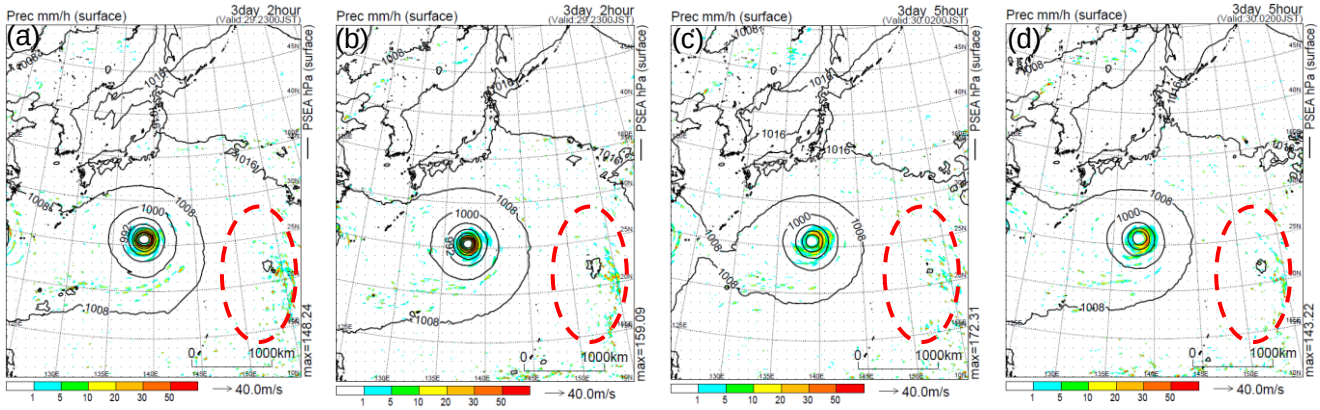

Figure 2 Horizontal distributions of hourly rainfall in (a) experiment A15 at 74 h, (b) A50 at 74 h, (c) C15 at 77h and (d) C50 at 77h.

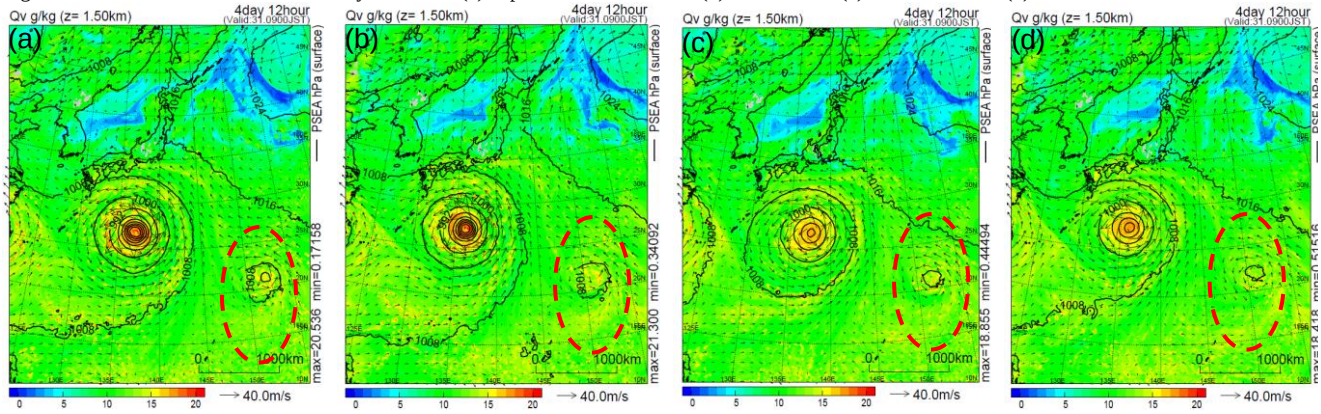

Figure 3Same as Fig.2 except for specific humidity (g/kg^{-1}) at 108 h.

Horizontal distributions of hourly rainfall indicate that a tropical depression appeared east-southeast of simulated Talas (Dashed red circle in Fig. 2a-d) for the first time of the lifecycle of the subsequent typhoon. A north-to-south sheared line of hourly rainfall appeared east of the tropical depression. The appearance time of the tropical depression in experiments C15 and C50 was three hours later than that in experiments A15 and A50. However, the location of the tropical depression little differed among the four experiments. The tropical depression was accompanied by environmental cyclonic circulation with a scale of a few hundred kilometers.

Figure 3 displays horizontal distributions of simulated specific humidity at 108 h at 1500 m height in all experiments. The amount of simulated specific humidity increased around the location of the subsequent typhoon in experiment A15 and tropical depression in the other experiments as the integration time went on. Simulated sea level pressure became low in experiment A15, while that was relatively high in the other experiments. This result suggests that the parameter of lateral boundary sponge layer affects intensification of the simulated tropical depression. In addition, simulated sea-level pressures in experiments C15 and C50 were higher than those in experiments A15 and A50 due to low simulated sea surface temperature beneath the tropical depression (not shown) and simulated specific humidity at 1500 m height around the depression, even though the environmental cyclonic circulation continuously appeared around the tropical-depression area.

This numerical study proposes the following genesis processes: environmental cyclonic circulation, an increase in specific humidity in the lower troposphere around a tropical depression within the environmental cyclonic circulation, and thereafter intensification of the circulation. Firstly, areas of high hourly rainfall (Fig. 2) and specific humidity in the lower troposphere (Fig. 3) scattered within a larger cyclonic circulation. Secondly a tropical depression intensified, shrinking the vortex. Sea surface cooling induced by preceding Talas is considered to suppress the increase in specific humidity in the lower troposphere, resulting in delaying of intensification of the subsequent tropical depression. In addition, this study shows that changes of atmospheric environments do affect the genesis process mentioned above through the results of the sensitivity experiments associated with lateral boundary conditions. Since the track simulations drastically changes, how sea surface cooling and lateral boundary condition affect the track simulation will be a subject in the future.

Acknowledgement

This work was supported by the Japan Society for the Promotion of Science (JSPS), Grant-in-Aid for Scientific Research (C) (22540454) and on Innovative Areas (Research in a proposed research area) (23106505).

References

Taylor, P. K., and M. J. Yelland (2001), The dependence of sea surface roughness on the height and steepness of the waves. *J. Phys. Oceanogr.*, **31**, 572-590.

Usui, N., S. Ishizaki, Y. Fujii, H. Tsujino, T. Yasuda, and M. Kamachi (2006), Meteorological Research Institute multivariate ocean variational estimation (MOVE) system: Some early results. *Advances in Space Research*, **37**, 896-822.

Wada, A., N. Kohno and Y. Kawai (2010), Impact of wave-ocean interaction on Typhoon Hai-Tang in 2005, *SOLA*, **6A**, 13-16.

Wada (2012), Oceanic influences for a large eye of Typhoon Talas in 2011. *Activ. Atmos. Oceanic. Modell.* **42**, 9.09-9.10.